RSC Advances

PAPER

Cite this: *RSC Adv.*, 2015, **5**, 36634

Exceptional thermal stability of undoped anatase TiO_2 photocatalysts prepared by a solvent-exchange method†

Igor Krivtsov,*[ab] Marina Ilkaeva,[ac] Viacheslav Avdin,[bc] Zakariae Amghouz,[d] Sergei A. Khainakov,[d] José R. García,[a] Eva Díaz[e] and Salvador Ordóñez[e]

Received 19th January 2015
Accepted 16th April 2015

DOI: 10.1039/c5ra01114k

www.rsc.org/advances

A new solvent-exchange technique to prepare anatase nanoparticles with exceptional thermal stability and photocatalytic activity is described here. The process of preparation is accomplished by using organic solvents to precipitate hydrous titania particles from a basic aqueous medium containing a titanium peroxo complex. Undoped titanium dioxide formed *via* a solvent exchange method has unprecedented thermal stability against transformation to the rutile phase, as opposed to TiO_2 prepared by the common method of the gelation of an aqueous titanium peroxo complex. On the basis of X-ray thermodiffraction experiments, it has been established that the thermal treatment at 1000 °C of the titania prepared by ethanol precipitation contains 100% pure anatase phase. The stabilization of anatase is induced by the high defectiveness of the TiO_2 nanostructure, which is evidenced from band-gap energy estimation, PXRD and HRTEM studies. The prepared TiO_2 nanoparticles show an outstanding photocatalytic activity comparable to the commercial **Aeroxide P25** photocatalyst in the UV-assisted decomposition of methylene blue.

1. Introduction

Despite the large number of alternatives,[1] titanium dioxide is considered to be the most appropriate semiconductor photocatalyst, because it is inexpensive, non-toxic and thermally stable according to many comprehensive reviews.[2–11] Anatase, generally considered the most active phase for photocatalytic applications, is a metastable polymorph which usually transforms into the stable rutile phase in the temperature range of approximately 500–700 °C. The development of new methods tailored to prepare anatase with increased thermal stability up to the sintering temperature range is of great importance, not only for photocatalysis, but also in other emerging applications such as self-cleaning and antibacterial ceramic production.[12] There are two general procedures to stabilize anatase: doping TiO_2 with metal cations,[13] fluorine,[14] or sulfur,[15] and preparation of mixed TiO_2/M_xO_y oxides.[16,17] The most significant drawback of these methods is that the dopants reduce crystallinity of TiO_2, which increases the recombination rate of electron–hole pairs. However, the preparation of stable undoped anatase is also discussed in the literature. Wu *et al.*[18] found that the anatase phase, prepared from titanium isopropoxide in the presence of tetramethylammonium hydroxide, was stable up to 950 °C. They attributed the retardation of anatase-to-rutile phase transition to the formation of the rod-like crystals. Similar observation about the effect of crystallite size and morphology on the stability of anatase phase was reported by Mao *et al.*[19] Li *et al.*[20] showed that the formation of intermediate brookite phase would enhance the stability of anatase at high temperatures. Application of simple alkoxide-based sol–gel procedures using urea or formic acid as modifying agents also led to improved stability of the desired titania polymorph.[21,22] But recently, the emerging class of precursors based on peroxo complexes have been used for metal oxide synthesis.[23,24] Moreover, shape of anatase crystals was successfully controlled *via* hydrothermal treatment of titanium peroxo complexes.[25,26] Etacheri *et al.*[27] used peroxo titanic acid to prepare visible light active TiO_2 photocatalyst with 100% anatase phase after heat treatment at temperature as high as 900 °C.

Herein, we report a new facile solvent-exchange method for preparing TiO_2 nanoparticles. We have found that titanium peroxo complex is insoluble in ethanol and acetone, as a consequence, hydrous titania suspensions were precipitated using these solvents. The proposed technique does not require

[a]*Department of Organic and Inorganic Chemistry, University of Oviedo-CINN, 33006 Oviedo, Spain. E-mail: uo247495@uniovi.es; zapasoul@gmail.com; Tel: +34 684348116*

[b]*Nanotechnology Education and Research Center, South Ural State University, 454080, Chelyabinsk, Russia*

[c]*Department of Chemistry, South Ural State University, 454080 Chelyabinsk, Russia*

[d]*Servicios Científico-Técnicos, Universidad de Oviedo, 33006 Oviedo, Spain*

[e]*Department of Chemical and Environmental Engineering, University of Oviedo, 33006 Oviedo, Spain*

† Electronic supplementary information (ESI) available: Additional data: XRD, EELS spectra, N_2 physisorption data, SEM and TEM analyses. See DOI: 10.1039/c5ra01114k

utilization of toxic, unstable and volatile alkoxide precursors as well as complex organic structure-directing agents or templates. Thus, it can be considered as an environmentally friendly approach for preparing high performance titania photocatalysts. The prepared TiO_2 nanoparticles exhibit temperatures of anatase-to-rutile phase transformation higher than those previously reported.[15,18,21,22,27]

2. Experimental

2.1 Chemicals

Titanium oxysulfate hydrate containing not more than 17% of H_2SO_4, as well as 30 wt% hydrogen peroxide (H_2O_2) water solution were purchased from Aldrich. Ammonium hydroxide 20% water solution, ethanol and acetone (all VWR Chemicals) were of analytical grade and used as received without additional purification. The commercial photocatalyst **Aeroxide P25** (Degussa P25) was purchased from Aldrich. The concentration of titanium oxysulfate was determined gravimetrically prior to its use in synthesis. Titanium oxysulfate has been chosen as precursor due to its high stability under ambient conditions, which is not the case for titanium tetrachloride or titanium alkoxides.

2.2 Synthesis

Firstly, titanium hydroxide was precipitated from 25 mL of 0.2 M titanium oxysulfate solution in sulfuric acid by addition of 3 M NH_3 aqueous solution, the final pH of precipitate was 9.0. Then, it was centrifuged at 7000 rpm and washed with deionized water until a negative reaction for sulfate ions was achieved. The aqueous titanium peroxo complexes were synthesized by addition of 4 mL of 30 wt% hydrogen peroxide to the precipitates and gradual adjustment of the pH value of the reaction mixture to 9.5 by adding ammonia. Finally, clear bright yellow stable solutions were formed and their volumes were adjusted to 25 mL. The solutions were cooled in an ice bath in order to prevent fast decomposition of H_2O_2, as well as evaporation of ethanol and acetone. The cooled solutions of titanium peroxo complexes were mixed with equal volumes of ethanol or acetone. The mixed solutions became turbid immediately, because the hydrous titania particles were formed. The obtained suspensions were left for 24 h and then centrifuged at 8000 rpm for 5 min, after that the pale-yellow precipitates were isolated and washed several times with water. For the sake of comparison, the sample prepared in the absence of any organic solvents was also investigated. Because the aqueous solution of titanium peroxo complex synthesized as mentioned above was stable, it was heated at 50 °C for 2 h in order to induce titanium hydrolysis and precipitation of peroxo titanate gel. The samples prepared by (i and ii) isolation of hydrous titania with ethanol or acetone and (iii) gelation of aqueous complex solution were designated as **TiEt**, **TiAc** and **TiAq**, respectively. All precipitates were dried at 70 °C for 24 h before subjecting to investigation. Also the samples were thermally treated in a muffle furnace at specific temperatures (500 °C, 800 °C, 900 °C and 1000 °C) with a heating rate of 5 °C min^{-1} and left for 30 min at each specific temperature before cooling down.

2.3 Characterization

Powder XRD patterns were registered on a Rigaku Ultima IV diffractometer, using Ni-filtered CuK_α radiation source. The PXRD data were refined, where unit cell parameters and anatase phase content were estimated using MAUD software and crystal sizes were calculated by Scherrer equation for anatase (101) reflection. Thermodiffraction analysis was carried out using the X'pert Pananlytical diffractometer for **TiEt** sample calcined at 400 °C for 2 h prior to measurement. **TiEt** was heated up to 1000 °C at a heating rate of 5 °C min^{-1} and the XRD patterns were collected every 30 min during 5 h at this temperature. A Shimadzu UV-2700 spectrophotometer with integrated sphere attachment was used to obtain diffuse reflectance (DR) spectra of the samples using barium sulfate as a reference. Band gap energy was estimated by Kubelka–Munk method. Bruker Tensor 27 spectrometer was used to collect FTIR spectra. Thermal analysis were carried out by means of NETZSCH 449C simultaneous TG/DTA analyzer at a heating rate of 10 °C min^{-1} under air flow. SEM images were obtained by using JEOL JSM-7001F field emission scanning electron microscope equipped with EDX detector; the samples were gold-coated prior to observation. The EDX analysis confirmed the absence of sulfur in the TiO_2 samples. A Micromeritics ASAP 2020 was used to obtain N_2 adsorption–desorption isotherms at 77 K. Before the experiment, the samples were outgassed under vacuum at 400 °C. Surface area and pore volume were calculated using BET and BJH methods. TEM, HRTEM, selected area electron diffraction (SAED), nanobeam electron diffraction (NBD), and EELS (electron energy loss spectroscopy) studies were performed on a JEOL JEM-2100F transmission electron microscope operated at an accelerating voltage of 200 kV, equipped with a field emission gun (FEG) and an ultra-high resolution pole-piece that provided a point-resolution better than 0.19 nm. The samples for TEM were dispersed in ethanol, sonified and sprayed on a Holey carbon film coated copper grid and then allowed to air-dry, finally, Gatan SOLARUS 950 was used before observation.

2.4 Photocatalytic activity test

Synthesized titania materials were tested in the aqueous-phase photocatalytic decomposition of methylene blue (**MB**) in a stirred batch reactor. For the experiments, 25 mg of each sample previously calcined in air at 500 °C, 800 °C and 1000 °C for 30 min was placed into a quartz reactor. Later, 50 mL of **MB** aqueous solution (20 mg L^{-1}) was added to the catalyst. Before irradiation, the suspension was magnetically stirred in the dark until the adsorption equilibrium was reached in 30 min. Afterward, the suspension was exposed to ultraviolet irradiation. The UV-light source was 500 W lamp (Helios Italquartz) having maximum emission at 365 nm and equipped with a water-cooling jacket. The reactor with suspension was positioned at a distance of 50 cm from the lamp, which gives a light intensity of 16 mW cm^{-2}. The suspension was constantly stirred during the UV-irradiation and 5 mL aliquots were taken every 30 min during 240 min. The solution was separated from the catalyst using a centrifuge, and the concentration was determined photometrically by the absorbance at 664 nm using a

Perkin Elmer Lambda 20 spectrophotometer. After that, the solution, together with the catalyst powder were returned back into the reactor and irradiation has continued. Photolysis of the **MB** solution in the absence of catalyst was carried out under the same experimental conditions. It was found that only 1.5% of **MB** was decomposed under these conditions.

3. Results and discussion

All the as-synthesized samples were found to be amorphous (see ESI, Fig. S1†), except **TiAq** sample that shows a broad peak centered at $2\theta = 9.2^{\circ}$ on the XRD pattern, which was attributed to the ammonia peroxo titanate complex.[28] FTIR spectra (Fig. 1) of the as-prepared samples reveal some differences in the structural features of the precipitates. The most intense band at 1385 cm^{-1} confirms the presence of ammonia in all the samples. The intense and well-defined band at 900 cm^{-1}, observed in the spectrum of the peroxo titanate gel (**TiAq**), corresponds to the stretching O–O vibrations, while the peak at 696 cm^{-1} indicates the presence of Ti–O–O bonds. However, the bands corresponding to the peroxo groups are not clearly seen in **TiAc** and **TiEt** spectra. A similar observation was made by Liao *et al.*[26] when the solvothermal method is applied to synthesize TiO_2 from the mixture of peroxo titanate complex and organic solvent. We suppose that the reaction between organic solvents and peroxo groups has caused the decomposition of the latter, which in turn, led to the oxolation of hydrous titania species. The broad absorption band centered at 616 cm^{-1} in **TiAc** and **TiEt** spectra is attributed to Ti–O–Ti stretching vibrations, this is most likely due to the very high degree of condensation of oxo-species in these precipitates. Likewise, the decomposition of peroxo groups while preparing the **TiAc** and **TiEt** samples is also evidenced by DR-UV-vis spectroscopy study (Fig. S2†). The **TiAq** sample absorbs light in the visible region due to the presence of peroxo groups on titania. Contrarily, the visible light absorbance is considerably decreased in the case of the **TiAc** and **TiEt** samples (Fig. S2†). Moreover, this method provides additional information about structural features of titania particles and coordination state of titanium. The sharp absorption peak at 219 nm in **TiAq** spectrum can be attributed to the charge transfer process in isolated TiO_4 units.[29] The shifting of absorbance bands towards longer wavelengths

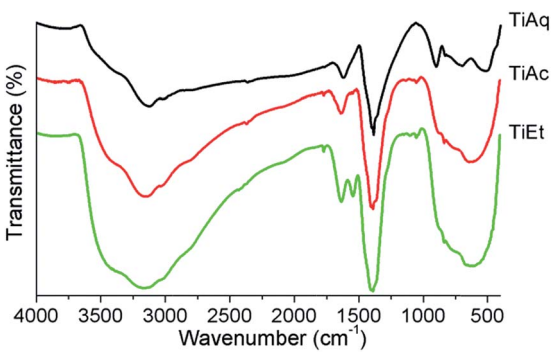

Fig. 1 FTIR spectra of the as-synthesized samples.

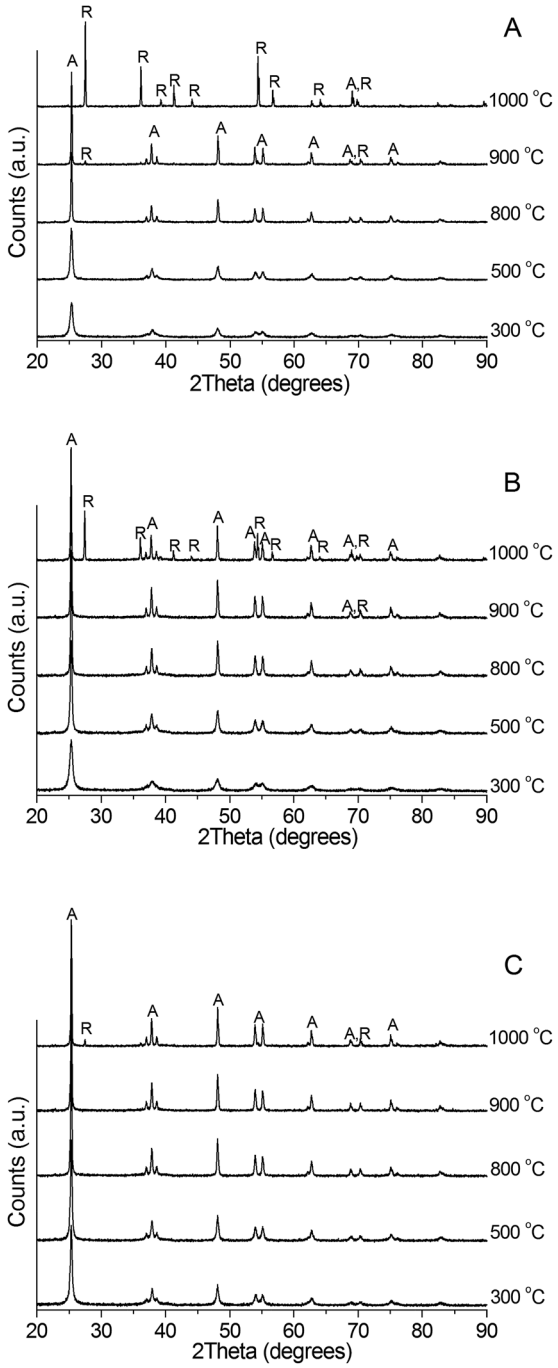

Fig. 2 Powder XRD patterns of (A) **TiAq**, (B) **TiAc** and (C) **TiEt** samples treated at different temperatures in a muffle furnace, where A indicates reflections of anatase phase and R for rutile.

indicates the presence of large titania particles. The absorbance bands at 334 nm in the **TiEt** and **TiAc** spectra suggest that these samples show more condensed TiO_2 phase compared to **TiAq** sample. Thermal analysis of the as-synthesized samples was carried out in order to determine the temperatures for the elimination of volatile components and exothermic effects associated with phase transitions. Thermal decomposition of **TiAq** is similar to that one reported previously.[28] The DTA curve shows one endothermic and three well-defined exothermic

Table 1 The results of powder XRD analysis and band gap energy estimation

Sample	T (°C)	Unit cell parameters (Å)		Crystal size (nm)	Anatase : rutile ratio (wt%)	Band gap energy (eV)
		a	c			
TiAq	500	3.785(4)	9.508(4)	22	100 : 0	3.02
	800	3.782(2)	9.525(2)	49	100 : 0	3.15
	900	3.783(1)	9.534(1)	49	96 : 4	
	1000				0 : 100	2.93
TiAc	500	3.785(2)	9.507(4)	29	100 : 0	3.24
	800	3.785(2)	9.516(1)	41	100 : 0	3.30
	900	3.785(4)	9.518(1)	52	100 : 0	
	1000	3.782(1)	9.517(1)	64	69 : 31	3.20
TiEt	500	3.784(4)	9.503(4)	31	100 : 0	3.23
	800	3.784(4)	9.509(2)	44	100 : 0	3.32
	900	3.784(3)	9.513(1)	48	100 : 0	
	1000	3.783(1)	9.516(2)	76	96 : 4	3.24

peaks corresponding to the elimination of adsorbed and chemically bonded water, decomposition of peroxo groups and crystallization process of amorphous titania (Fig. S3a†). However, thermal decomposition of **TiAc** and **TiEt** samples prepared *via* solvent-exchange method is different (Fig. S3b and c†). Similarly to **TiAq** sample, there are three exothermic peaks on the DTA curves for **TiAc** and **TiEt**, but unlike the **TiAq** sample, the first two exothermic peaks observed at low temperature correspond to the combustion process of the organic residue. The as-prepared samples start to crystallize around 300 °C and with further heat treatment their crystallinity increases (Fig. 2). The results of XRD analysis are summarized in Table 1. Titania sample **TiAq** prepared from the aqueous peroxo titanate gel has the lowest thermal stability among all samples, however, its stability is much higher than TiO_2 prepared *via* conventional non-peroxo techniques.[27] Rutile phase is detected in the **TiAq** sample after treatment at 900 °C and the complete anatase-to-rutile transition takes place at 1000 °C. The **TiAc** sample is more stable, it contains pure anatase phase after being subjected to 900 °C for 30 min. Furthermore, titania prepared by solvent-exchange method using ethanol (**TiEt**) shows a remarkably higher stability, it retains 96 wt% of anatase phase even after heat treatment in muffle furnace at temperature as high as 1000 °C. In order to investigate the process of anatase-to-rutile transformation *in situ*, X-ray thermodiffraction study was performed for **TiEt** sample (Fig. 3a). It shows that the **TiEt** sample possesses unprecedented stability towards formation of rutile phase, it retains 60 wt% of anatase phase after being treated at 1000 °C for 5 h (Fig. 3b). The slight controversy observed in the percentage of rutile phase, when **TiEt** sample is thermally treated in muffle furnace or during the thermodiffraction experiment, is attributed to overheating of the sample in the furnace, which leads to the formation of 4% of rutile phase after 30 min, while 150 min in the diffractometer heating chamber was necessary to reach the same percentage of transformation. According to XRD data, we cannot attribute the hindering of anatase-to-rutile phase transformation to the crystallite size effect, because the differences in this parameter are insignificant. The differences in the *c*-axis lattice parameter indicate that crystalline anatase formed from **TiAc** and **TiEt** precursors contains higher concentration of defects than that prepared from **TiAq** one. The above hypothesis is corroborated

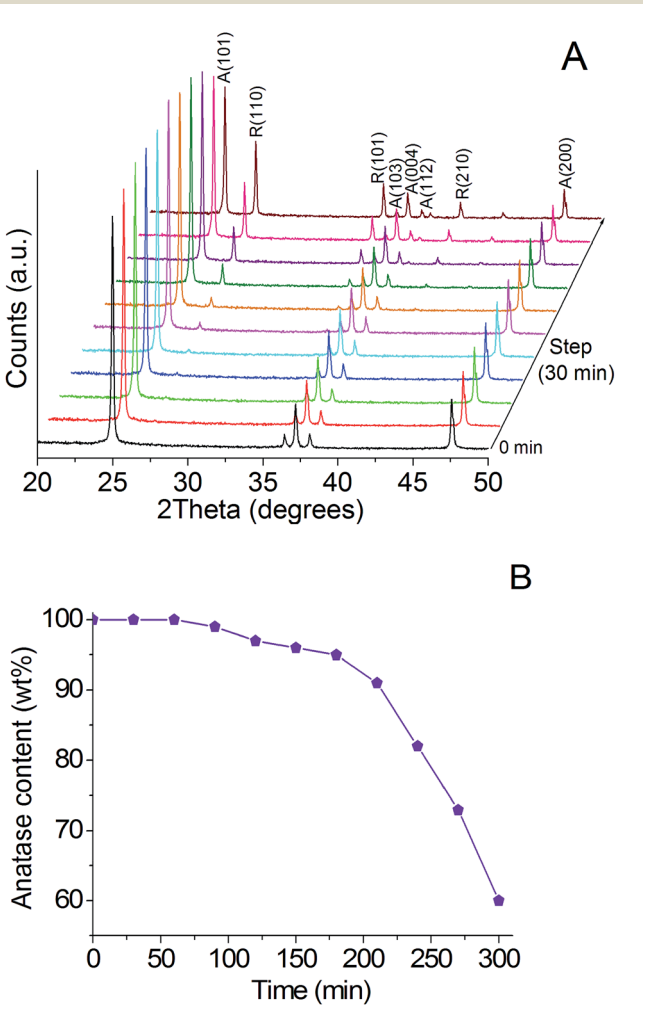

Fig. 3 **TiEt** sample at 1000 °C: (A) HT-pXRD patterns as a function of the treatment time (the pXRD scans were taken every 30 min) and (B) changes in anatase/rutile content.

by the results of band-gap (BG) energy estimation (Table 1). Usually BG energy of anatase TiO_2 is 3.2 eV, however, this value varies depending on the presence of dopants and degree of crystallinity. Like Etacheri *et al.*[27] we observe the band gap shrinkage when TiO_2 anatase is prepared *via* aqueous titanium peroxo complex route (**TiAq**). It can be attributed to the nitrogen-doping effect in the samples calcined not higher than 500 °C, as the presence of nitrogen is evident from the EELS data (Fig. S4†). After thermal treatment at 800 °C its BG value increases, but it is still less than 3.2 eV, due to the presence of oxygen vacancies formed on sites of the removed N atoms (Table 1). However, **TiAc** and **TiEt** samples obtained by solvent-exchange route show broader BG, even though nitrogen-doping occurring when they are treated at 500 °C, and then no nitrogen is detected at calcination temperatures higher than 800 °C (Fig. S4†). This indicates high concentration of defects in the structure, and it also means that nitrogen-doping could play some noticeable role, but cannot be solely responsible for the defects formation at elevated temperatures. The formation of defects is likely to be due to rapid loss of ligands, *i.e.* peroxo groups, which are not stable in organic solvents. This leads to fast assembling process of the oxide network. On the contrary, the aqueous peroxo titanate gel containing peroxo groups is stable up to high temperatures,[30] and because peroxo groups hinder the condensation of titania species, the crystallization rate becomes slow. As a result, less defective structure is formed. TEM and HRTEM images and electron diffraction (ED) patterns of pure anatase **TiAq** and **TiEt** samples calcined at 800 °C are shown in Fig. 4 and 5. Both samples show the presence of crystal grains with the average size of *ca.* 45 nm and 50 nm for **TiEt** and **TiAq** (Fig. 4a–d and S5†), respectively, in agreement with the results obtained from XRD analysis. From a careful inspection of SAED patterns (Fig. 4e and f) and NBD patterns for individual crystal grains (Fig. 4g and h), the degree of crystallinity seems to be similar for both samples and all ED patterns have been indexed as anatase phase. No detectable traces of rutile phase have been found by indexing the ED patterns. TEM images reveal mesoporous crystal grains with pore diameters in the range 3–12 nm in the case of **TiEt** sample (Fig. 5a). HRTEM images displayed in Fig. 5c–f for both samples show an interplanar spacing of 0.35 nm corresponding to (101) atomic planes. Several line defects, such as dislocations, along the (101) plane have been observed in the case of **TiEt** (Fig. 5c and e), while very distinguishable planar defects, such as grain boundaries, are manifested in the case of **TiAq** (Fig. 5b and f). Obviously, the blurred lattice fringes observed in HRTEM images in the case of **TiEt**, such as Fig. 5e, are an indication of the defects induced from the lattice distortion, probably attributed to the crystallization process. EELS spectra for **TiAq** and **TiEt**, are shown in Fig. S6.† Because of the octahedral coordination of Ti atoms, the L3 and L2 edges are then both subdivided into two edges by the strong crystal-field splitting arising from the surrounding O atoms.[31] The splitting of Ti L2, 3 edges is slightly higher in **TiAq**, which may reflect that the local octahedral coordination is weakly present in the case of **TiEt**, probably due to the degree of crystallinity and/or the structural defects as confirmed by HRTEM study. The splitting of O–K edge with a separation of 2.4 eV for **TiAq** and **TiEt** (Fig. S6†) confirms the anatase phase.[32] TEM and SEM images of **TiAq** calcined at 800 °C (Fig. 4b and d and S7a†) show the presence of sintered oxide composed of large densely packed grains, while the images of **TiEt** (Fig. 4a and c and S7c†) show unagglomerated TiO_2 grains and with the increase of calcination temperature leads to the formation of densely packed large particles (Fig. S7d†).

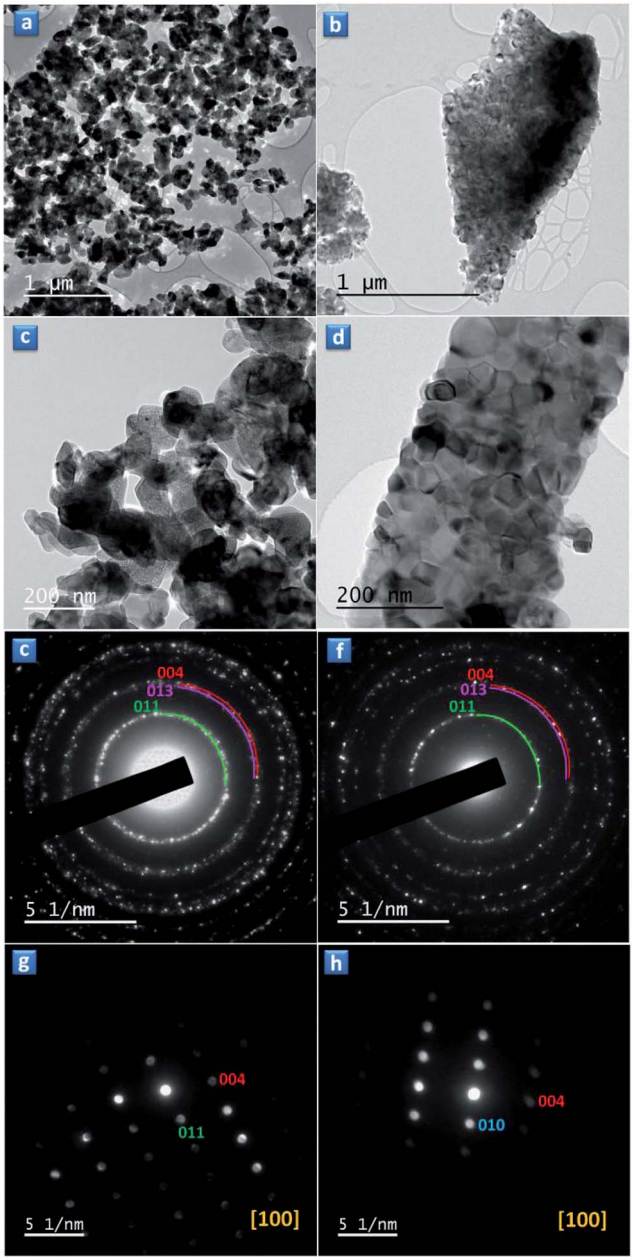

Fig. 4 (a–d) TEM images, (e and f) selected area electron diffraction (SAED) and (g and h) nanobeam electron diffraction (NBD) for **TiEt** (left) and **TiAq** (right) thermally treated at 800 °C.

TiEt sample exhibit high photocatalytic activity for the decomposition of **MB** when compared to **TiAc** and **TiAq** samples calcined at 500 °C (Fig. S8†). The crystallinity of TiO_2 is improved after calcination at higher temperatures (Table 1),

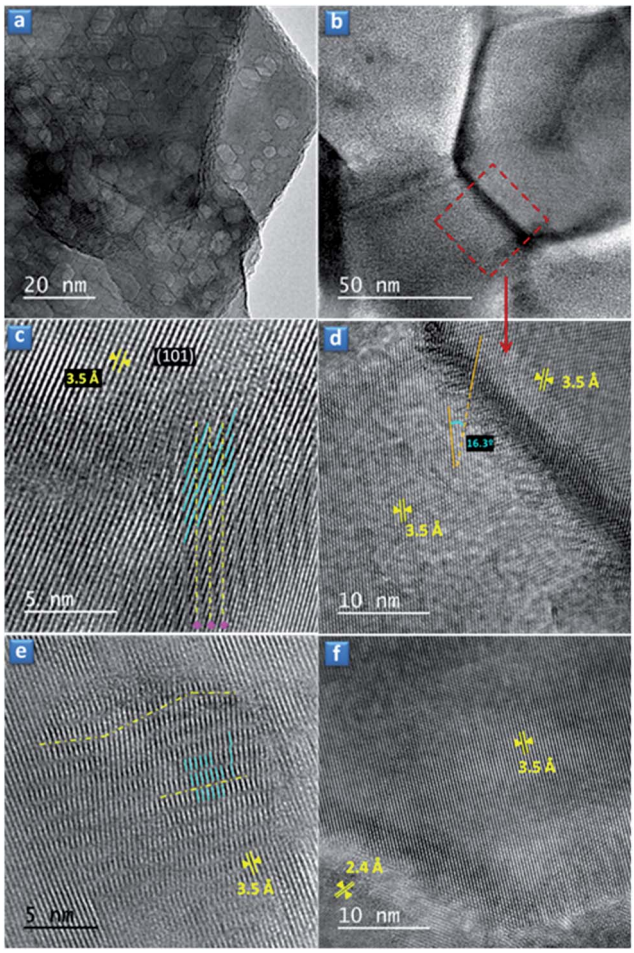

Fig. 5 TEM and HRTEM images of **TiEt** (a, c and e) and **TiAq** (b, d and f) samples calcined at 800 °C. The dislocations observed in **TiEt** are indicated by cyan lines and directions of slip are indicated by yellow dashed lines.

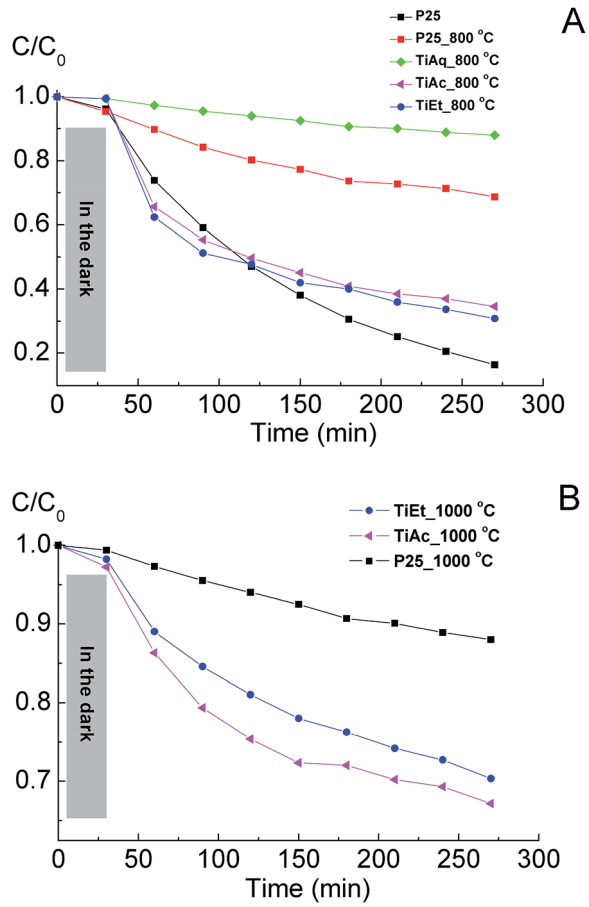

Fig. 6 Decomposition of **MB** under UV radiation in the presence of **TiAq**, **TiAc** and **TiEt** samples synthesized in this work, compared with **Aeroxide P25**, as a function of the calcination temperature: (A) 800 °C and (B) 1000 °C.

this fact may lead to enhancement of photocatalytic activity. Despite the crystallinity of **TiAq** sample is improved by thermal treatment at 800 °C, this sample does not show any increase of photocatalytic activity, which is probably attributed to its densification and therefore resulting in low BET surface area of just 9 $m^2\ g^{-1}$ (Fig. S9†). However, **TiEt** sample treated at the same temperature retains higher surface area (34 $m^2\ g^{-1}$) and mesopore volume (Fig. S10†). The decomposition rates of **MB** in the presence of **TiEt** or **TiAc** samples calcined at 800 °C reach almost the values obtained by the commercial photocatalyst **Aeroxide P25** (Fig. 6a). This known commercial photocatalyst has proved to be very efficient; however it shows poor thermal stability compared to **TiEt** and **TiAc** samples. The calcination of **Aeroxide P25** at temperatures higher than 800 °C induced the full transition from anatase phase to the photocatalytic less-active rutile phase (Fig. S11†). Obviously, 100% pure anatase phase up to 900 °C, high surface area and mesoporosity of **TiEt** and **TiAc** samples are the main contributors to the outstanding photocatalytic activity (Fig. 6a). When **TiEt** and **TiAc** are thermally treated at 1000 °C, their photodecomposition rate of **MB** decreases. However, their photocatalytic activity is still nearly twice higher than for **Aeroxide P25** treated at the same temperature (Fig. 6b). Moreover, the degree of **MB** photodegradation in **TiAc** sample was slightly enhanced compared to **TiEt**, which could be attributed to the better charge separation on the anatase–rutile interface.[33,34]

4. Conclusion

In summary, we have developed and described a new solvent-exchange method for the preparation of undoped TiO_2 photocatalysts with unprecedented anatase thermal stability and outstanding photocatalytic activity. We have succeeded in preparing mesoporous pure anatase TiO_2 nanoparticles which are stable up to 1000 °C. The preparation procedure is completed by using ethanol to precipitate hydrous titania particles from basic medium containing titanium peroxo complex. High thermal stability against anatase-to-rutile phase transformation is caused by the defectiveness of the formed TiO_2 structure, which is the consequence of the rapid decomposition of titania peroxo species. The photocatalytic activity of the prepared TiO_2 materials, thermally treated at temperatures higher than 800 °C, is superior to the commercial **Aeroxide P25**

photocatalyst treated at the same conditions. The thermal stability of anatase up to the sintering temperatures, along with its high photocatalytic activity, offer new possibilities to prepare a wide range of self-cleaning and anti-bacterial TiO_2-based ceramic materials to meet medical and domestic needs.

Acknowledgements

We gratefully acknowledge financial support from the Spanish MINECO (MAT2013-40950-R, CTQ2011-29272-C04-02, and Técnicos de Infraestructuras Científico-Tecnológicas grants PTA2011-4903-I to Z.A. and PTA2011-4950-I to S.A.K.), the Government of the Principality of Asturias (Severo Ochoa PhD grant BP-14-029 to M. I.) and FEDER. South Ural State University acknowledges financial support of The Ministry of Education and Science of the Russian Federation Grant no. 16.2674.2014/K.

References

1 M. D. Hernández-Alonso, F. Fresno, S. Suárez and J. M. Coronado, Development of Alternative Photocatalysts to TiO_2: Challenges and Opportunities, *Energy Environ. Sci.*, 2009, **2**, 1231–1257.

2 X. Lang, W. Ma, C. Chen, H. Ji and J. Zhao, Selective Aerobic Oxidation Mediated by TiO_2 Photocatalysis, *Acc. Chem. Res.*, 2014, **47**, 355–363.

3 A. Kubacka, M. Fernández-García and G. Colon, Advanced Nanoarchitectures for Solar Photocatalytic Applications, *Chem. Rev.*, 2012, **112**, 1555–1614.

4 X. B. Chen and S. S. Mao, Titanium Dioxide Nanomaterials: Synthesis, Properties, Modifications, and Applications, *Chem. Rev.*, 2007, **107**, 2891–2959.

5 M. R. Hoffmann, S. T. Martin, W. Choi and D. W. Bahnemann, Environmental Applications of Semiconductor Photocatalysis, *Chem. Rev.*, 1995, **95**, 69–96.

6 A. A. Ismail and D. W. Bahnemann, Mesoporous titania photocatalysts: preparation, characterization and reaction mechanisms, *J. Mater. Chem.*, 2011, **21**, 11686–11707.

7 D. J. Stacchiola, S. D. Senanayake, P. Liu and J. R. Rodriguez, Fundamental Studies of Well-Defined Surfaces of Mixed-Metal Oxides: Special Properties of MOx/TiO_2(110) {M = V, Ru, Ce, or W}, *Chem. Rev.*, 2013, **113**, 4373–4390.

8 W. Y. Teoh, J. A. Scott and R. Amal, Progress in Heterogeneous Photocatalysis: From Classical Radical Chemistry to Engineering Nanomaterials and Solar Reactors, *J. Phys. Chem. Lett.*, 2012, **3**, 629–639.

9 M. Cargnello, T. R. Gordon and C. B. Murray, Solution-Phase Synthesis of Titanium Dioxide Nanoparticles and Nanocrystals, *Chem. Rev.*, 2014, **114**, 9319–9345.

10 K. Liu, M. Cao, A. Fujishima and L. Jiang, Bio-Inspired Titanium Dioxide Materials with Special Wettability and Their Applications, *Chem. Rev.*, 2014, **114**, 10044–10094.

11 L. Liu and X. Chen, Titanium Dioxide Nanomaterials: Self-Structural Modifications, *Chem. Rev.*, 2014, **114**, 9890–9918.

12 M. Machida, K. Norimoto and T. Kimura, Antibacterial Activity of Photocatalytic Titanium Dioxide Thin Films with Photodeposited Silver on the Surface of Sanitary Ware, *J. Am. Ceram. Soc.*, 2005, **88**, 95–100.

13 J. Choi, H. Park and M. R. Hoffmann, Effects of Single Metal-Ion Doping on the Visible-Light Photoreactivity of TiO_2, *J. Phys. Chem. C*, 2010, **114**, 783–792.

14 S. C. Padmanabhan, S. C. Pillai, J. Colreavy, S. Balakrishnan, D. E. McCormack, T. S. Perova, Y. Gun'ko, S. J. Hinder and J. M. Kelly, A Simple Sol–Gel Processing for the Development of High-Temperature Stable Photoactive Anatase Titania, *Chem. Mater.*, 2007, **19**, 4474–4481.

15 P. Periyat, S. C. Pillai, D. E. McCormack, J. Colreavy and S. J. Hinder, Improved High-Temperature Stability and Sun-Light-Driven Photocatalytic Activity of Sulfur-Doped Anatase TiO_2, *J. Phys. Chem. C*, 2008, **112**, 7644–7652.

16 M. Hirano, K. Ota and H. Iwata, Direct Formation of Anatase (TiO_2)/Silica SiO_2) Composite Nanoparticles with High Phase Stability of 1300 °C from Acidic Solution by Hydrolysis under Hydrothermal Condition, *Chem. Mater.*, 2004, **16**, 3725–3732.

17 J.-Y. Kim, C.-S. Kim, H.-K. Chang and T.-O. Kim, Effects of ZrO_2 Addition on Phase Stability and Photocatalytic Activity of ZrO_2/TiO_2 Nanoparticles, *Adv. Powder Technol.*, 2010, **21**, 141–144.

18 J. Wu, S. Hao, J. Lin, M. Huang, Y. Huang, Z. Lan and P. Li, Crystal Morphology of Anatase Titania Nanocrystals Used in Dye-Sensitized Solar Cells, *Cryst. Growth Des.*, 2008, **8**, 247–252.

19 Y. Mao and S. S. Wong, Size- and Shape-Dependent Transformation of Nanosized Titanate into Analogous Anatase Titania Nanostructures, *J. Am. Chem. Soc.*, 2006, **128**, 8217–8226.

20 W. Li, Y. Bai, C. Liu, Z. Yang, X. Feng, X. Lu, N. K. Van der Laak and K. Y. Chan, Highly Thermal Stable and Highly Crystalline Anatase TiO_2 for Photocatalysis, *Environ. Sci. Technol.*, 2009, **43**, 5423–5428.

21 S. C. Pillai, P. Periyat, R. George, D. E. McCormack, M. K. Seery, H. Hayden, J. Colreavy, D. Corr and S. J. Hinder, Synthesis of High-Temperature Stable Anatase TiO_2 Photocatalyst, *J. Phys. Chem. C*, 2007, **111**, 1605–1611.

22 N. T. Nolan, M. K. Seery and S. C. Pillai, Spectroscopic Investigation of the Anatase-to-Rutile Transformation of Sol–Gel-Synthesized TiO_2 Photocatalysts, *J. Phys. Chem. C*, 2009, **113**, 16151–16157.

23 J.-Y. Piquemal, E. Briot and J.-M. Bregeault, Preparation of Materials in the Presence of Hydrogen Peroxide: from Discrete or "Zero-Dimensional" Objects to Bulk Materials, *Dalton Trans.*, 2013, 29–45.

24 M. Kakihana, M. Kobayashi, K. Tomita and V. Petrykin, Application of Water-Soluble Titanium Complexes as Precursors for Synthesis of Titanium Containing Oxides *via* Aqueous Solution Process, *Bull. Chem. Soc. Jpn.*, 2010, **83**, 1285–1308.

25 N. Murakami, Y. Kurihara, T. Tsubota and T. Ohno, Shape-Controlled Anatase Titanium(IV) Oxide Particles Prepared by Hydrothermal Treatment of Peroxo Titanic Acid in the Presence of Polyvinyl Alcohol, *J. Phys. Chem. C*, 2009, **113**, 3062–3069.

26 J. Liao, L. Shi, S. Yuan, Y. Zhao and J. Fang, Solvothermal Synthesis of TiO_2 Nanocrystal Colloids from Peroxotitanate Complex Solution and Their Photocatalytic Activities, *J. Phys. Chem. C*, 2009, **113**, 18778–18783.

27 V. Etacheri, M. K. Seery, S. J. Hinder and S. C. Pillai, Oxygen Rich Titania: A Dopant Free, High Temperature Stable, and Visible-Light Active Anatase Photocatalyst, *Adv. Funct. Mater.*, 2011, **21**, 3744–3752.

28 H. Ichinose, M. Terasaki and H. Katsuki, Synthesis of peroxo-modified anatase sol from peroxo titanic acid solution, *J. Ceram. Soc. Jpn.*, 1996, **104**, 715–718.

29 G. N. Vayssilov, Structural and Physicochemical features of titanium silicalites, *Catal. Rev.*, 1997, **39**, 209–251.

30 M. Ilkaeva, I. Krivtsov, V. Avdin, S. Khainakov and J. R. Garcia, Comparative Study of Structural Features and Thermal Behavior of Mixed Silica-Titania Xerogels Prepared *via* the Peroxo Method and the Conventional Co-Precipitation Technique, *Colloids Surf.*, 2014, **456**, 120–128.

31 M. Okada, P. Jing, Y. Yamada, M. Tazawa and K. Yoshimura, Low-Energy Electron Energy Loss Spectroscopy of Rutile and Anatase TiO_2 Films in the Core Electron Excitation Regions, *Surf. Sci.*, 2004, **566–568**, 1030–1034.

32 A. Gloter, C. Ewels, P. Umek, D. Arcon and C. Colliex, Electronic Structure of Titania-Based Nanotubes Investigated by EELS Spectroscopy, *Phys. Rev. B: Condens. Matter Mater. Phys.*, 2008, **80**, 035413.

33 D. O. Scanlon, C. W. Dunnill, J. Buckeridge, S. A. Shevlin, A. J. Logsdail, S. M. Woodley, C. R. A. Catlow, M. J. Powell, R. G. Palgrave, I. P. Parkin, G. W. Watson, T. W. Keal, P. Sherwood, A. Walsh and A. A. Sokol, Band Alignment of Rutile and Anatase TiO_2, *Nat. Mater.*, 2013, **12**, 798–801.

34 D. C. Hurum, A. G. Agrios, K. A. Gray, T. Rajh and M. C. Thurnauer, Explaining the Enhanced Photocatalytic Activity of Degussa P25 Mixed-Phase TiO_2 Using EPR, *J. Phys. Chem. B*, 2003, **107**, 4545–4549.